Nanoscale

Accepted Manuscript

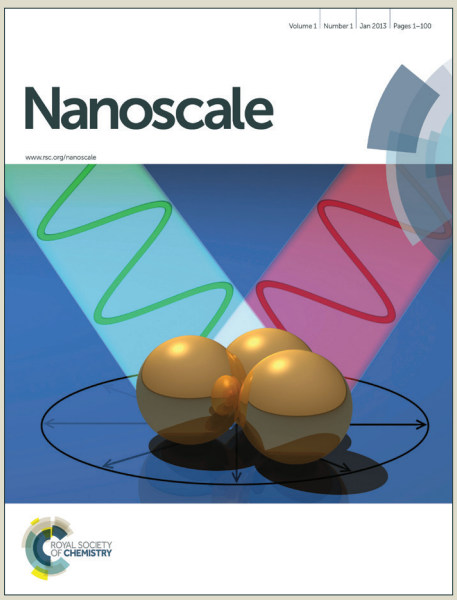

ROYAL SOCIETY OF CHEMISTRY

www.rsc.org/nanoscale

The synthesis of TiO_2 nanotubes with ZnO nanoparticles to possess antibacterial properties with no stem cell toxicity

Wenwen Liu[a, b, c], Penglei Su[b], Su Chen[a], Na Wang[a], Yuanping Ma[a], Yiran Liu[a], Jinshu Wang[b], Zhenting Zhang*[a], Hongyi Li**[,b] and Thomas J. Webster***[,c, d]

a. Laboratory of Biomaterials and Biomechanics, Beijing Key Laboratory of Tooth Regeneration and Function Reconstruction, School of Stomatology, Capital Medical University, Tian Tan Xi Li No. 4, Beijing, 100050, China

b. Photoelectrochemical Research Group, Key Laboratory of Advanced Functional Materials, School of Materials Science and Engineering, Beijing University of Technology, Beijing, 100124, China

c. Chemical Engineering Department, Northeastern University, Boston, MA, 02115, USA

d. Center of Excellence for Advanced Materials Research, King Abdulaziz University, Jeddah, Saudi Arabia

* Corresponding author. Tel./fax: +86 10 67099279.

** Corresponding author. Tel./fax: +86 10 67391101.

***Corresponding author. Tel: (617) 373-2989, fax: (617) 373-2209

E-mail addresses: veromcawen@gmail.com (W. Liu), lhy06@bjut.edu.cn (H. Li), zztttxl@hotmal.com (Z. Zhang), th.webster@neu.edu (T.J. Webster)

Abstract: To provide titanium (Ti) with antibacterial properties, different concentrations of zinc oxide (ZnO) nanoparticles were decorated on anodized titanium dioxide (TiO_2) nanotubes by a simple hydrothermal treatment method. The particle sizes of ZnO, which were evenly distributed and tightly adherent on the walls of the Ti nanotubes, ranged from 20-50 nm. Results from this study showed that Zn was released from the TiO_2 nanotubes in a constant, slow, and biologically-inspired manner. Importantly, results showed that the ZnO decorated TiO_2 nanotubular samples inhibited *Streptococcus mutants* and *Porphyromonas gingivalis* growth compared to control unmodified Ti samples. Specifically, *S. mutants* and *P. gingivalis* growth were both reduced 45%-85% on the ZnO decorated Ti samples compared to Ti controls after 7 days of culture. When examining the mechanism of action, it was further shown for the first time that the ZnO decorated Ti samples inhibited the expression of *Streptococcus mutans* bacteria adhesive genes. Lastly, results showed that the same samples which decreased bacteria growth the most (the 0.015M precursor $Zn(NO_3)_2$ samples), maintained similar mesenchymal stem cell growth compared to Ti controls for up to 7 days. In summary, results from this study showed that compared to plain TiO_2 nanotubes, TiO_2 decorated with 0.015M ZnO provided unprecedented antibacterial properties while maintaining a stem cell proliferative capacity necessary for enhancing the use of Ti in numerous medical applications, particularly in dentistry.

Keywords: Titania nanotubes; Zinc oxide; Antibacterial; *Streptococcus mutans*; *Porphyromonas gingivalis*

Introduction

Titanium (Ti) has been widely used in bone tissue engineering applications for decades (such as for dental and orthopedic applications). [1] Titania (TiO_2) forms on the surface of Ti in oxygen containing environments (such as the body) and has been shown to have suitable cytocompatibility properties but no inherent antibacterial properties. [2] Bacteria infection is a main reason for dental/orthopedic implant failure. [3] Infection is the major reason causing short (less than 5 years) dental/orthopedic implant functional lifetimes. [4] It is, therefore, crucial that to improve the functional lifetime of Ti-based medical devices, one must incorporate antibacterial properties into today's Ti. However, it is not trivial to identify an approach that will reduce bacteria growth without reducing mammalian cell functions.

Mimicking the same natural hierarchical nano-structured surface features present on bone on TiO_2 may provide natural antibacterial properties to Ti to improve its use in numerous orthopedic applications. [5-9] TiO_2 nanotubes (TNTs) prepared by anodizing Ti under unique conditions have been reported to have a great potential in numerous drug delivery applications to fight against bacterial infections. [8] Specifically, to provide antibacterial properties to Ti, some studies have doped antibacterial agents (such as gentamycin) into TNTs to inhibit bacterial proliferation. Several studies have reported that incorporating polymers, drugs or specific elements into nanotubular structures anodized into TiO_2 may be a strategy worth pursuing.[9-13] However, such techniques to date are limited by drug loading capacity, and drug release rates, as the incorporated antibacterial agents in TNTs have short release times. Moreover, it has been well documented that bacteria are quickly developing a resistance to the numerous antibacterial drugs that we have developed to kill them.[14,15]

Thus, in order to provide extended antibacterial properties to TiO_2, which do not involve the use of antibacterial pharmaceutical agents, some metallic elements have been added into TNT, such as silver (Ag) [16-19] and copper (Cu). [20,21] However, many of these elements are quite toxic to mammalian cells. For its use in Ti, the required Ag dose should be low (0.2 ppm) which may not be enough for the prolonged resistance of bacterial growth.[22] Moreover, Cu can be easily eroded and oxidized to eliminate such antibacterial properties. [23]

Similar to Ag and Cu, but without the concern of high toxicity, zinc (Zn) possesses antibacterial effects and osteogenic properties.[24] Due to their increased surface area and, thus, exposure of Zn, ZnO nanoparticles have even more special properties. Owing to the small size and large specific surface area of nanoparticles, ZnO exhibits

unique physico-chemical properties that may differ from their bulk micron counterparts. [25] Moreover, the nano size of ZnO increases the possibility of bacteria uptake. Due to this, some studies have hence reported that ZnO nanoparticles are more toxic to bacteria than their micron equivalents.[26,27]

Herein, the above two approaches using TNTs and ZnO nanoparticles were combined to reduce bacteria growth on Ti-based medical devices. ZnO nanoparticles were decorated onto and into TNTs by a novel hydrothermal method. Hexagonal particles of ZnO at different concentrations in TNT were fabricated and used to determine their antibacterial properties. Importantly, some research has reported high levels of mammalian cell functions and an osteogenic inducing ability of Zn.[24,28,29] Results from this study provided much promise for adding ZnO nanoparticles to TNTs to reduce bacteria growth (without the use of antibiotics) while maintaining stem cell growth. Moreover, the present *in vitro* study also provided the first genetic reasons for the observed reduced bacterial growth on ZnO nanoparticles decorated onto and into Ti_2O nanotubes, which should be useful in future studies to optimize its antibacterial properties.

Results and discussion

Substrate characterization

Results showed that the diameter of the TNTs was about 70 nm and the length was about 2 μm (Figures 1 and 2) with ZnO nanoparticles incorporated well into the TNTs. The different concentrations of the decorated ZnO are shown in the SEM images of the TNT-Zn samples and all the ZnO nanoparticles were of hexagonal flake geometry. The AFM images showed that the surfaces of pure Ti, TNT and TNT-Zn0.015 all had similar roughness (Figures 3 and Table 2). TNT-ZN0.015 was used as a representative example for all TNT-Zn samples.

Chemical composition and crystal structure

Results of this study further showed that the ratio of Ti to O for TNT was about 1 : 2 (Table 1). For all the ZnO decorated samples, the Zn element was detected. As expected, the Zn ion total content from the samples increased along with increased concentrations of Zn $(NO_3)_2$. ICP results showed the total ZnO content and the content rates of Zn^{2+} were further confirmed in the XRF results (Table 2). EDS results showed that the Zn content in the TNT-Zn0.03 and TNT-Zn0.075 samples was greater than the other two samples. Elemental Zn was homogeneously distributed on the sample surface. (Table 1)

Table 1. Energy-dispersive X-ray Spectrometry (EDS) Results

sample [a]	Ti		O		Zn	
	weight ratio	atomic	weight ratio	atomic	weight ratio	atomic

		ratio		ratio		ratio
TNT	61.99	35.26	38.01	64.74	0.00	0.00
TNT-Zn0.005	60.26	35.8	34.91	62.09	4.83	2.1
TNT-Zn0.015	51.2	30.59	35.58	63.63	13.22	5.79
TNT-Zn0.03	34.97	26.54	31.05	54.57	33.98	18.89
TNT-Zn0.075	30.14	21.84	25.06	54.37	44.8	23.79

[a] TNT: TiO_2 nanotube, TNT-Zn: Zn-decorated TNTs with four different concentrations of $Zn(NO_3)_2$:0.005M, 0.015M, 0.03M, and 0.075M.

Table 2. X-Ray Fluorescence (XFR) Spectrometry and Inductively Coupled Plasma Atomic Emission (ICP-AES) Spectrometry Results for the Zn decorated samples.

Sample [a]		XRF	ICP (ppm, total Zn ion)
TNT-Zn0.005	Ti	98.37%	
	Zn	1.63%	3.298
TNT-Zn0.015	Ti	97.94%	
	Zn	2.06%	6.196
TNT-Zn0.030	Ti	95.84%	
	Zn	4.16%	16.49
TNT-Zn0.075	Ti	88.92%	
	Zn	11.08%	33.98

[a] TNT: TiO_2 nanotube, TNT-Zn: Zn-decorated TNTs with four different concentrations of $Zn(NO_3)_2$:0.005M, 0.015M, 0.03M, and 0.075M.

The XRD spectra of the samples displayed Ti and anatase TiO_2 peaks for the TNT and TNT-Zn0.015 samples (Figure 4). The corrosion characteristics of titanium with amorphous and anatase nanotubes in Hank's solution have been tested before and it was found that the nanotube layers, especially the anatase nanotubes, exhibited better corrosion resistance than smooth-Ti.[30] Corrosion resistance is an important aspect regarding the survival rate of endosseous implants. The metal element combined with a TiO_2 nanotube can enhance corrosion resistance.[31] Thus, the material in this study has the strong potential (in terms of reduced corrosion) to be used for dental implant applications.

Here, TNT-ZN0.015 was used as a representative example for all the TNT-Zn samples. Some small peaks of rutile phase were also detected in the XRD of TNT and TNT-Zn0.015. The TNT-Zn0.015 sample had slight changes in XRD but there were no feature peaks for the ZnO compounds; most likely this is because the content of ZnO was too low to be detected by XRD.

Further XPS studies revealed that Ti, O, and Zn peaks were found for all the ZnO decorated samples (Figure 5a). The C signals are most likely present due to contamination. The distribution of ZnO in TNT (Sample TNT-Zn0.015) was investigated using the XPS depth profile (Figure 5b). TNT-ZN0.015 was used as a representative

example for all TNT-Zn samples. The XPS spectra of elemental Zn from TNT-Zn0.015 showed that energies of the Zn 2p3 peak at 1021.7 eV and 1044.8 eV were assigned to Zn 2p1 and did not shift with the depth of investigation. The binding energy of Zn 2p3/2 peak is located at 1021.7 eV, a perfect fit with Zn^{2+} in ZnO. This result indicated that ZnO was embedded into the TiO_2 nanotubes, which is critical for creating a prolonged release of Zn^{2+} for decreasing bacteria growth. As was achieved here, the ZnO embedded dose in TNTs can be adjusted using precursors containing different concentrations of $Zn(NO_3)_2$. Both the EDS and XPS spectra demonstrated that ZnO could be introduced into TiO_2 nanotubes using the presently designed approach.

Contact angle and surface energy measurements

There were significant differences in both water contact angles and, thus, surface energies for the samples of interest to this study (Table 3). Here, it was observed that the surface modification of TiO_2 with nanotubes improved hydrophilicity compared to plain Ti. Further, it was found that the surface energy decreased (i.e., hydrophilicity decreased) with the addition of ZnO nanoparticles to TNTs. This decrease was not as obvious when concentrations of the $Zn(NO_3)_2$ precursor were below 0.015 M. For concentrations of the $Zn(NO_3)_2$ precursor below 0.015M, the surface energy was still higher than that of plain Ti. The results of the contact angle tests revealed that the surface energy of TiO_2 increased after anodization. The surface energy of TNT decorated with ZnO nanoparticles was slightly smaller than that of TNT, however, it was still higher than that of the control (unanodized) Ti.

Table 3. Water Contact Angles, Total Surface Energy and Roughness of the Samples.

Sample [a]	Contact angle (°)			Surface energy (mJ/m^2)	Roughness (μm)
	Water	Diiodomethane	Ethylene glycol		
Ti	73.3±1.5	48.3±2.3	55.0±1.7	38.9±1.9	0.257±0.029
TNT	16.0±1.3	16.7±2.0	23.3±1.4	53.8±1.7	0.169±0.024
TNT-Zn0.005	34.2±2.6	27.0±2.1	28.0±2.3	50.2±2.4	0.120±0.020
TNT-Zn0.015	44.8±1.8	30.3±1.7	42.3±2.0	48.7±1.8	0.123±0.006
TNT-Zn0.030	46.5±3.1	40.3±2.1	55.0±2.6	43.6±2.4	0.108±0.011
TNT-Zn0.075	83.8±4.3	72.3±2.7	70.3±1.9	23.9±2.6	0.133±0.006

[a] Ti: Titanium, TNT: TiO_2 nanotube, TNT-Zn: Zn-decorated TNTs with four different concentrations of $Zn(NO_3)_2$:0.005M, 0.015M, 0.03M, and 0.075M.

Zn^{2+} embedding and release

Results from this study showed that the amounts of Zn^{2+} released followed the order TNT-Zn0.075 > TNT-Zn0.03 > TNT-Zn0.015 > TNT-Zn0.005 (Figure 6 a, b). However, all of the samples decorated with ZnO nanoparticles exhibit the same release rate of Zn, indicating well Zn^{2+} releasing capability. The accumulated amount

increased steadily during the first 9 days. As expected, the amount of Zn^{2+} released diminished with time.

Antibacterial activity

Results of this study showed that for *S. mutans*, the TNT and TNT-Zn0.005 had no influence on bacteria functions at all time points (Figure 7a, b). However, the TNT-Zn0.075 had greater antibacterial effectiveness than plain Ti especially after days 5 and 7. The antibacterial properties of TNT-Zn0.015 and the TNT-Zn0.030 were no different compared to each other and both of them demonstrated exceptional antibacterial properties compared to plain Ti.

For *P. gingivalis*, the antibacterial properties were similar for the TNT-Zn0.015, TNT-Zn0.030 and TNT-Zn0.075 groups, all better than plain Ti. The TNT-Zn0.005 had higher antibacterial activity than TNT but it was not significant at the statistical threshold for the current study. Compared to plain Ti, the reduction of bacteria at all time points for TNT-Zn0.015, TNT-Zn0.030, and TNT-Zn0.075 were about 40-85%. MTT assays matched the results of the colony count assays (Figure 8 a, b).

Further, antibacterial properties were investigated with SEM (Figures 9 and 10). *S. mutans* formed a biofilm on the plain Ti samples with long chain-shaped intact bacteria membranes on the surface of TNT. The membranes were rough and the fission was unclear for the *S. mutans* on TNT-Zn0.005, TNT-Zn0.015 and TNT-Zn0.030 samples. The cells were damaged and the membrane became corrugated on the TNT-Zn0.075 surface. For *P. gingivalis*, the cells formed colonies on the untreated Ti. The cells looked smooth and were intact with rod-shapes on TNT. The shape of *P. gingivalis* changed along with increased ZnO incorporated in the TNT-Zn samples. The amounts of bacteria continued to decrease with an increase in ZnO in the TNT-Zn.

Lastly, the ability of the TNT-Zn samples to prevent bacteria growth was determined by fluorescence microscopy (Figures 11 and 12). After 24 h of culture, *S. mutans* biofilms formed and adhered on Ti, TNT and TNT-Zn0.005 samples. There were more *S. mutans* alive on the plain Ti than the others. The amount of the live *S. mutans* on the surface of TNT-Zn 0.015 and TNT-Zn0.03 was similar. There were a few live *S. mutans* on the surface of TNT-Zn 0.075. For *P. gingivalis*, the amount of live cells in the media decreased with the increasing incorporation of ZnO onto and into the TNT samples.

This study clearly demonstrated that the different concentrations of ZnO exhibited different antibacterial ability. The antibacterial effect was stable during the first 7 days, which is consistent with the Zn^{2+} release profiles. All of the decorated ZnO samples had stable release rates. There was no large (potentially toxic) release at the beginning of

the immersion. This property imitates a slow-release effect of elements in saliva, blood or other tissue fluid environments. Daily Zn^{2+} release from all samples were lower than 3.62 ppm, which has been reported to have no cytotoxicity to mammalian cells. [32]

The ZnO decorated samples had a better antibacterial effect on the adhesive bacteria than planktonic bacteria. *S. mutans* can adhere on a dental implant abutment directly. This antibacterial effect is partly ascribed to the bacterial toxicity contributed by Zn^{2+} release. There are also sequential oxidation-reduction reactions, which occur at the ZnO particle surface to produce reactive species such as hydrogen peroxide (H_2O_2) and hydroxyl radicals. The reactive oxygen species (ROS) might trigger membrane lipid per-oxidation and cause an antibacterial effect.[33] Reactive oxygen species also cause intracellular oxidative stress, cell membrane damage and DNA damage. [34, 35] Raghupathi reported that ROS may not be the only factor for the antibacterial activity of ZnO nanoparticles according to genetic analysis, which suggests that small sized ZnO nanoparticles lead to an increase in cell death, probably due to disruption of the bacterial cell wall.[36] However, most oral bacteria are anaerobic or facultative anaerobic bacteria. The ROS generated due to the incorporation of ZnO may have more of an effect on oral bacteria.

P. gingivalis can adhere on other bacteria or the acquired saliva pellicle. In this research, the ROS concentration may have been greater and more effective on the surface adhesive bacteria than on the planktonic bacteria. The nano ZnO and TNT surface morphology may also have more directly inhibited *S. mutans* than *P. gingivalis*. On the other hand, ZnO has more of an antibacterial effect on gram-positive bacteria than gram-negative bacteria. [37-39] Thus, the decorated ZnO samples had better of an antibacterial effect on *S. mutans* than *P. gingivalis,* which is significant for clinical applications. In dental implants, the inhibition of initial bacterial adhesion can slow or decrease further pathogenic bacterial attachment.

***S. mutans* adhesion-associated gene expression**

A down regulation of the gtf B, C and D genes were observed for the TNT-Zn0.015 and TNT groups (Figure 13). All the three bacteria adhesion - associated genes were lower for TNT-Zn0.015 than for the other TNT groups. *S. mutans* is one of the most important pathogens in the human oral system, whose main virulence property is the ability to adhere to the teeth or dental implants. *S. mutans* can mediate *P. gingivalis* infection by producing extracellular glucans from dietary carbohydrates.[40] Periodontitis can induce peri-implantitis which is predominantly comprised of *P. gingivalis*.[41] Thus, weakening or eliminating the adhesion virulence of *S. mutans* is the first step for antibacterial research. *S. mutans* produces glucosyltransferases (GTFs) which is an extracellular enzyme leading to

the adherence and encoded by gtf B, gtf C and gtf D. The GTFs have been recognized as virulence factors in the pathogenesis of dental caries, which catalyze the formation of soluble and insoluble glucans to the dental plaque matrix polysaccharide composition. [42] In this study, the expression of gtf genes on different materials showed that the TNT-Zn0.015 inhibited gtf genetic expression. Especially for gtf D genetic expression, TNT-Zn0.015 had less than a 0.5 fold change than the control group. Kooh [43] reported that 0.1mM Zn^{2+} can down-regulate gtfC and gtfD expression of *S.mutans* and reduce the insoluble glucan synthesis by *S. mutan*. [44] The gtf B and gtf C genes are in an operon-like arrangement and encode GTF-I and GTF-SI enzymes that mostly produce water-insoluble-(1-3)-linkedglucans, whereas the gtfD gene encodes GTF-S that synthesizes water-soluble-(1-6)-linked glucans.[45] The water-soluble glucans require the presence of water-insoluble glucans to provide full adhesion.[42] Thus, gtf D had a lower expression in the TNT-Zn0.015 group which can be interpreted as having an improved effect on inhibiting *S. mutan* adhesion. The bacterial response was influenced by the intrinsic physical-chemical superficial properties of the materials. [40] Zn^{2+} has the capacity to enhance proton permeability of bacterial cell membranes and acts to diminish ATP synthesis in glycolyzing cells and reduces F-ATPase activity, which appears to be substrate-limited in *S. mutans*. [46] Zn^{2+} also inhibits the secretion of enzymes, and thereby reduces the production of GTFs involved in the synthesis of insoluble glucan. [44] Thus, Zn^{2+} released from ZnO is one of the most effective elements for invoking antibacterial properties.

Stem cell proliferation

Stem cell proliferation (Figure 14) was significantly lower for the TNT-Zn0.030 and TNT-Zn0.075 samples than that for any other groups, thus, helping to identify a concentration of ZnO inhibitory or toxic to stem cells. In fact, after days 4 and 7, cells died on the TNT-Zn0.030 and TNT-Zn0.075 samples. In contrast, stem cell proliferation was significantly higher on control Ti and TNT-Zn0.015 samples than all samples with higher ZnO concentrations after 7 days of culture. Coupled with the previous results, such results identified that TNT-Zn0.015 maximized antibacterial properties while maintaining stem cell growth.

Cell morphology

The stem cells spread on pure Ti after 1-day of culture (Figure 15). On the surface of TNT-Zn0.015, the stem cells had a polygonal morphology and more vinculin cell membrane protein expression than other samples. Some of the cells shrunk and agglomerated on the TNT-Zn0.030 and TNT-Zn0.075 samples with poorly expressed vinculin and non-uniform morphologies.

Results demonstrated that the ZnO decorated TNTs were cytocompatible to stem cells at certain concentrations (less than the TNT-Zn0.015 samples and the concentration of the precursor $Zn(NO_3)_2$ at 0.015M). In this study, the TNT-ZnO0.015 sample contained the proper ZnO to balance an antibacterial effect and stem cell compatibility. After 1, 4 and 7 days, cells on the TNT, TNT-Zn0.005 and TNT-Zn0.015 samples had similar trends of proliferation. Various kinds of physical stresses from the substrate morphology and topography can accelerate stem cell differentiation into a specific cell lineage, which will have to be the focus of future studies. [47] Results from this study showed that the stem cells proliferated less on the higher ZnO decorated TNT samples than on the control group, however, stem cell proliferation was the same on the TNT-ZnO0.015 compared to controls demonstrating its selection as the best material in this study. From the fluorescence images, red actin cytoskeleton staining showed that the TNT-ZnO0.015 elicited stem cell elongation, which induced cytoskeletal stress and promoted stem cell expansion.[48] Vinculin was highly expressed on the TNT-Zn0.0.015, which distributed along the edge of the cell and filopodia. Vinculin plays a key role in cytoskeletal development and cellular focal adhesion. [49] Thus, the results here exhibited that stem cells preferred TNT-Zn0.015 compared to all other groups.

Lastly, we have seen that the present samples can be recycled and retain their antibacterial properties. Specifically, we have observed that after ultrasonically cleansing and sterilization, the samples still maintain their original antibacterial properties and stem cell compatibility.

Materials and methods

Sample preparation and characterization

Preparation of TiO_2 nanotubes (TNT)

Pure titanium sheets (Aldrich, 10×10×0.3 mm^3) were ultrasonically washed with acetone, ethylalcohol and deionized water for 10 min, sequentially. Anodization was carried out in a two-electrode electrochemical cell where Ti sheets served as the working electrode and a graphite sheet served as the counter electrode at 20 ^oC. The electrolyte was ethylene glycol containing 0.3 wt% ammonium fluoride (NH_4F) and 2 vol% distilled water. After anodization at 30 V for 2h, TNTs were formed on the Ti sheets. The control group was pure titanium (Ti). All samples were ultrasonically cleaned and annealed at 450 ^oC for 3 h in air to transform the amorphous TNTs phase into an anatase crystalline structure which has higher corrosion resistance and better biocompatibility than amorphous TNTs.

Incorporation of ZnO nanoparticles into TNTs

The annealed TNTs samples were immersed into an aqueous solution containing zinc nitrate ($Zn(NO_3)_2$) and hexamethylenetetramine ($(CH_2)_6N_4$) at a 1:2 molar ratio. Then, 2 mg of citric acid was added into the solution. The samples were separated into four different concentrations of $Zn(NO_3)_2$:0.005M, 0.015M, 0.03M, and 0.075M and then were hydrothermally reacted at 70 ^oC for 2h to form all of the ZnO-decorated TNTs (termed TNT-Zn). Lastly, all samples were rinsed with deionized water, dried and annealed at 300 ^oC for 100 min before in vitro experiments. All samples were sterilized in an autoclave at 120 ^oC for 40 min.

Characterization of samples

The surface morphologies of pure Ti, TNTs and TNT decorated with ZnO were observed using field-emission scanning electron microscopy (SU8000 Series UHR Cold-Emission FE-SEM, Hitachi, Japan) and atomic force microscopy (AFM, Auto-Probe CP, Park Scientific Instruments, USA). The samples were further characterized by taking cross sections of the samples and analyzing them with transmission electron microscopy (TEM, JEM2100F, Japan). Their phase compositions were analyzed by X-ray diffraction (XRD, Philips X' Pert Pro, USA). The elemental composition and distribution of ZnO were measured by energy-dispersive X-ray spectrometry (EDS, Hitachi, Japan). The bonding states of the surface constituents were identified by X-ray photoelectron spectroscopy (XPS, ESCALAB MK-II, UK).

Zn ion release and TNT incorporating capacity

The amounts of Zn^{2+} released from the TNT-Zn samples were monitored by soaking them in phosphate buffered saline (PBS). The samples were immersed in 4 ml of PBS for 9 days. The released Zn^{2+} concentrations in PBS at different time points (1, 3, 5, 7, and 9 days) were determined by inductively coupled plasma atomic emission spectrometry (ICP-AES, Vista AX, Varian, USA). The time points were chosen to coincide with the antibacterial tests to be described. The Zn^{2+} content in the different samples was determined with an X-Ray Fluorescence Spectrometer (XRF，X-Supreme8000, USA) and ICP-AES. Samples were measured by XRF and then dissolved in 1% HF and 1.5% HNO_3 for the ICP-AES experiments.

Contact angle and surface roughness analysis

Contact angle (CA) measurements on control and experimental samples were carried out with a contact analysis system (Model OCA20, Dataphysics Co., Ltd).[50] The surface free energy was obtained by measuring the contact angle with the aid of the test fluids whose surface energy is known. Distilled water, diiodomethane and ethylene glycol were used as the test fluids. Based on the surface energy parameters of these different liquids,

surface energy was calculated according to previously described methods. [50-51]

The surface roughness of the samples was measured by a surface profiler (EKTAK-XT profiler, Bruker) at a 2 mm scan distance and a scan rate of 0.2 mm / s. The scan was performed three times at different places on each sample. The Ra values were reported as the mean ± standard deviation.

Antibacterial assays

Bacteria cultures

The ability of the proposed materials to reduce bacterial growth was evaluated using *Streptococcus mutans* (*S. mutans*, UA159) and *Porphyromonas gingivalis* (*P. gingivialis*, ATCC33277). *S. mutans* were cultured in tryptic soy broth (TSB) or agar (TSA) plates. *P. gingivalis* were cultured in a Center for Disease Control and Prevention (CDC) anaerobic blood base medium. To determine the adhesion of the bacteria on the proposed materials, each sample was incubated in 4 ml of the *S. mutans* suspension at a concentration of 10^8 cfu ml^{-1}. All samples were placed in the *S. mutans* suspension containing media at 37 ^oC in a micro-aerobic environment (80%N_2, 10%CO_2, and 10%H_2) for 48h. At the end of the incubation period, the samples were gently rinsed thrice with phosphate-buffered saline (PBS, pH7.4) in order to remove non-adherent *S. mutans*. The adherent *S. mutans* on each sample were detached into 4ml of TSB by ultrasonic vibration (40W) for 2 min and were serially diluted using 10-fold steps with sterile physiological saline. Then, 200 µl of the diluted *S. mutans* suspension was inoculated onto TAS agar plates. After incubation for 48h at 37 ^oC, bacteria were counted. The samples were ultrasonically cleaned, sterilized and re-incubated as described above. Each sample was repeatedly incubated 3 more times. The adherent *S. mutans* were counted after 2, 4, 6 and 8 days on the same sample. *P. gingivalis* were also used in a similar manner to that just described.

The antibacterial rates (R) for the adherent *S. mutans* and the planktonic *P. gingivalis* in the medium were calculated based on the following formula:

$$R = (A\text{-}B) / A \times 100\% \quad (1)$$

Where A presents the number of bacteria in the control group and B is the number of bacteria in the experimental group.

At the end of incubation, the *S. mutans* adhering to the surface were fixed and dehydrated as previously reported [32], followed by drying in a critical point dryer (EMS 850, Electro Microscopy Science Co., USA). The samples were sputtered with gold and observed using SEM.

To confirm the colony account assay, spectrophotometry measurements were carried out at 490 nm. Specifically, after 48 h of culture, all *S. mutans* which adhered on the samples and planktonic *P. gingivalis* were collected. All bacteria were diluted (1:10) in 1 ml medium. 100 µl of 3-(4,5-dimethylthiazol-2-yl)-2,5-diphenyltetrazolium bromide (5mg/ ml) (MTT, Sigma) were added to each group followed by incubation for 2 h (37 ^{o}C). Before spectrophotometry measurements, 200 µl of dimethylsulfoxide (DMSO) was added to collect the MTT chemicals.

Moreover, fluorescence microscopy was also used to determine bacteria functions on the samples of interest to the present study. For this, two kinds of bacteria were inoculated on the samples each at a concentration of 10^8 cfu ml^{-1} in TSA and CDC medium separately. After 24 h of incubation, the medium was removed and cells were stained using a Live/Dead® BacLight™ Kit (Invitrogen, USA) according to the manufacturer's instructions. The bacteria were observed using scanning confocal laser microscopy (CLSM, Olympus Fluo Viev FV1000; Germany). The kit contains SYTO 9 and Propidium Iodide (PI). The living cells appeared green (due to SYTO 9) while the dead cells were red (due to PI).

***S. mutans* adhesion-associated gene expression**

In a novel manner, to aid in determining the mechanism(s) by which the samples of interest to the present study influenced bacteria functions, bacteria gene expression was also determined here. For this, *S. mutans* were cultured on the samples at a concentration of 10^8 cfu ml^{-1} in 2ml of TSA and at a micro-aerobic environment at 37 ^{o}C. After 48h, the samples were rinsed with PBS for 3 times. The adhered *S. mutans* were detached using ultrasonication (CPS-1A, Shanghai, China) for 2 min in ice water. The *S. mutans* detached from the samples were collected and suspended in 1 ml of Trizol reagent (Invitrogen, Carlsbad, CA, USA). After 3 freeze-thaw cycles in Trizol, 200 µl of chloroform were added and the solution was shaken for 15s and then was rinsed for 3 min at room temperature. Then, the solution was centrifuged at 12000g for 15 min at 4 ^{o}C. The mixture was separated into the aqueous phase which contained the mRNA. 500 µl of the aqueous phase was transferred and mixed with 500 µl of isopropyl alcohol. Twenty minutes later, the mixed solution was centrifuged at 12000 g for 15 min at 4 ^{o}C. The RNA precipitated as an RNA pellet, which was then washed with 500 µl of 75% ethanol and centrifuged at 7500 g for 5 min at 4 ^{o}C. After redissolving the RNA in 50 µl DEPC water, the concentration of the RNA was calculated by UV spectrophotometry.

Reverse transcription was carried out using a M-MLV RTase Cdna Synthesis kit (Invitrogen) following the protocol in the kit. The primers for the gtfB, gtfC and gtfD genes used are shown in Table 1. The 16S rRNA gene was chosen as the internal standard for *S. mutans*. The reaction system included 3 μl of RNA, 1μl of random primer, DEPC treated water (9.5 μl), 5×PrimerScript™ Buffer (5 μl), dNTP (10mM) (5 μl), a Ribonuclease inhibitor (0.5μl), and M-MLV-RT (1 μl). After incubation for 60 min at 42 °C and 10 min at 70 °C, the cDNAs were added to the real-time PCR system. The real-time PCR was performed by the BioEasy SYBR Green Real-Time PCR kit (SUNBIO, China) in the Line-Gene Real-Time PCR Detection System (BIOER, Hangzhou, China). The mixture contained 10 μl of SYBR mix, cDNA (1.5 μl), 1 μl of forward and reverse primer (10 pmol / μl) and dd H_2O. The cycle was a 2 min initial denaturation at 94 °C. Then, 45 cycles at 94 °C were processed for 15 seconds and at 60 °C for 60 seconds. After the 72 °C cycle for 10 min, the critical threshold cycle (Ct) was recorded as the cycle. The fluorescence signal was read when the product was first detectable. The internal standard 16S rRNA gene from *S. mutans* was used to normalize the expression levels of all the target genes (Table 4). Relative mRNA abundance was determined by the $2^{-\Delta\Delta Ct}$ method.

Table 4. Primers for the S. *mutans* Target and Housekeeping Genes [a]

gene		primer	amplicon size (bp)
gtfB	F:	AGCAATGCAGCCAATCTACAAAT	96
	R:	ACGAACTTTGCCGTTATTGTCA	
gtfC	F:	CTCAACCAACCGCCACTGTT	91
	R:	GGTTTAACGTCAAAATTAGCTGTATTAGC	
gtfD	F:	CACAGGCAAAAGCTGAATTAACA	81
	R:	GAATGGCCGCTAAGTCAACAG	
16S	F:	CGGTCAGGAAAGTCTGGAGTAAA	120
	R:	TATCTACGCATTTCACCGCTACA	

[a] F, forward; R, reverse.

Stem cell proliferation assays

Bone mesenchymal stem cells (BMSCs) were extracted from the bone marrow of Sprague Dawley rats. BMSCs were cultured in Minimum Essential Medium α (MEM α, Gibico BRL, USA) with 10% fetal bovine serum (FBS, Gibico BRL, USA) and 1% penicillin / streptomycin (PS). The cells were cultured in a 5% CO_2 incubator at 37 °C and inoculated on the samples in 24-well plates at a density of 2×10^4 cells/well. After 1, 4 and 7 days of culturing, BMSC proliferation on the samples was investigated using the Cell Counting Kit-8 (CCK-8, Dongjing, Japan) according to manufacturer's instructions.

Stem cell morphology

BMSCs were seeded on the samples in 24-well plates at a density of 1×10^4 cells/well. After 24 h of incubation, the cells on the samples were fixed with 4% formaldehyde and treated with 1% Triton X-100. Then, fluorescence staining of the actin (cytoskeleton), vinculin (focal adhesion protein), and cell nucleus was performed with a triple staining. The samples were incubated with anti-vinculin mAb (V9264, Sigma) for 1 h. After washing three times in PBS, fluorescein isothiocyanate (FITC, F2562, Sigma) was added to the surfaces and incubated for 2 h. The cells were incubated with Alexa Fluor 594 Phalloidin (Invitrogen) for 30min and, at last, the cell nuclei were contrast-labeled by DAPI (Invitrogen) for 5 min. Cells were then observed using confocal laser scanning microscopy.

Statistical analysis

All experiments were conducted in triplicate. Statistically significant differences ($p<0.05$) were measured using a one-way ANOVA combined with the Student-Newman-Keuls (SNK) post-hoc test. Data were expressed as the mean ± standard deviation.

Conclusions

In summary, different concentrations of ZnO nanoparticles were decorated here onto and into TiO_2 nanotubes using a simple hydrothermal method. ZnO nanoparticles were distributed evenly along the entire length of the nanotube. The size and the quantity of the ZnO nanoparticles can be controlled by the precursor's concentration of the zinc nitrate ($Zn(NO_3)_2$) and hexamethylenetetramine ($(CH_2)_6N_4$). The ZnO decorated TiO_2 nanotube coatings inhibited both *S. mutans* and *P. gingivalis* and weakened the adhesion and virulence gene expression of *S. mutans*. Moreover, a suitable embedded ZnO concentration was identified among the different ZnO contents studied here. The results of this study suggest that it is possible to obtain both antibacterial properties while maintaining stem cell compatibility properties with a stable release of Zn^{2+} and the best sample for this was TNT-Zn0.015.

The slow and constant release of Zn ions is expected to provide antibacterial properties for preventing infection of the implant and at the same time provide stem cell compatibility. For these reasons, the ZnO decorated TNT materials have the potential to improve numerous dental applications, due to such novel antibacterial abilities (without using antibiotics) while retaining friendly stem cell compatibility.

Acknowledgements

This work was financially supported by the Beijing Natural Science Foundation (7132059), the National Outstanding Young Investigator Grant of China (51225402), and the Natural Science Foundation of China

(51002004, 81300916). HYL would also like to acknowledge the fellowship from China Scholarship Council, Rixin Talent authorized by Beijing University of Technology and Beijing Youth Talents.

Notes and reference

1. K. G. Neoh, X. Hu, D. Zheng and E. T. Kang, *Biomaterials*, 2012, **33**, 2813-2822.
2. K. C. Popat, L. Leoni, C. A. Grimes and T. A. Desai, *Biomaterials*, 2007, **28**, 3188-3197.
3. J. W. Costerton, P. S. Stewart and E. P. Greenberg, *Science*, 1999, **284**, 1318-1322.
4. J. Ata-Ali and F. Ata-Ali, *Int J Oral Maxillofac Surg*, 2013.
5. A. Dolatshahi-Pirouz, T. Jensen, D. C. Kraft, M. Foss, P. Kingshott, J. L. Hansen, A. N. Larsen, J. Chevallier and F. Besenbacher, *ACS Nano*, 2010, **4**, 2874-2882.
6. K. C. Popat, M. Eltgroth, T. J. Latempa, C. A. Grimes and T. A. Desai, *Biomaterials*, 2007, **28**, 4880-4888.
7. M. J. Dalby, N. Gadegaard, R. Tare, A. Andar, M. O. Riehle, P. Herzyk, C. D. Wilkinson and R. O. Oreffo, *Nat Mater*, 2007, **6**, 997-1003.
8. K. C. Popat, M. Eltgroth, T. J. LaTempa, C. A. Grimes and T. A. Desai, *Small*, 2007, **3**, 1878-1881.
9. M. Sinn Aw, J. Addai-Mensah and D. Losic, *Macromol Biosci*, 2012, **12**, 1048-1052.
10. M. Lai, K. Cai, L. Zhao, X. Chen, Y. Hou and Z. Yang, *Biomacromolecules*, 2011, **12**, 1097-1105.
11. Y. Xin, J. Jiang, K. Huo, T. Hu and P. K. Chu, *ACS Nano*, 2009, **3**, 3228-3234.
12. Y. H. Lee, G. Bhattarai, I. S. Park, G. R. Kim, G. E. Kim, M. H. Lee and H. K. Yi, *Biomaterials*, 2013, **34**, 10199-10208.
13. M. S. Aw, K. A. Khalid, K. Gulati, G. J. Atkins, P. Pivonka, D. M. Findlay and D. Losic, *Int J Nanomedicine*, 2012, **7**, 4883-4892.
14. G. M. Soares, L. C. Figueiredo, M. Faveri, S. C. Cortelli, P. M. Duarte and M. Feres, *J Appl Oral Sci*, 2012, **20**, 295-309.
15. J. M. ten Cate and E. Zaura, *Adv Dent Res*, 2012, **24**, 108-111.
16. M. M. Cortese-Krott, M. Münchow, E. Pirev, F. Hessner, A. Bozkurt, P. Uciechowski, N. Pallua, K. D. Kröncke and C. V. Suschek, *Free Radic Biol Med*, 2009, **47**, 1570-1577.
17. L. Zhao, H. Wang, K. Huo, L. Cui, W. Zhang, H. Ni, Y. Zhang, Z. Wu and P. K. Chu, *Biomaterials*, 2011, 5706-5716.
18. B. S. Necula, J. P. van Leeuwen, L. E. Fratila-Apachitei, S. A. Zaat, I. Apachitei and J. Duszczyk, *Acta Biomater*, 2012, **8**, 4191-4197.
19. S. Pal, Y. K. Tak and J. M. Song, *Appl Environ Microbiol*, 2007, **73**, 1712-1720.

20. K. Vasilev, V. Sah, K. Anselme, C. Ndi, M. Mateescu, B. Dollmann, P. Martinek, H. Ys, L. Ploux and H. J. Griesser, *Nano Lett*, 2010, **10**, 202-207.
21. L. Zhao, P. K. Chu, Y. Zhang and Z. Wu, *J Biomed Mater Res B Appl Biomater*, 2009, **91**, 470-480.
22. E. J. Park, J. Yi, Y. Kim, K. Choi and K. Park, *Toxicol In Vitro*, 2010, **24**, 872-878.
23. J. Park, S. Bauer, A. Pittrof, M. S. Killian, P. Schmuki and K. von der Mark, *Small*, 2012, **8**, 98-107.
24. K. Huo, X. Zhang, H. Wang, L. Zhao, X. Liu and P. K. Chu, *Biomaterials*, 2013, **34**, 3467-3478.
25. B. Wang, W. Y. Feng, M. Wang, T. C. Wang, Y. Q. Gu, M. T. Zhu, H. Ouyang, J. W. Shi, F. ;Zhang, Y. L. Zhao, Z. F. Zhai, H. F. Wang and J. Wang, *Journal of Nanoparticle Research*, 2008, **10**.
26. H. Yin, P. S. Casey, M. J. McCall and M. Fenech, *Langmuir*, 2010, **26**, 15399-15408.
27. J. Rousk, K. Ackermann, S. F. Curling and D. L. Jones, *PloS one*, 2012, **7**, e34197.
28. H. Zreiqat, Y. Ramaswamy, C. Wu, A. Paschalidis, Z. Lu, B. James, O. Birke, M. McDonald, D. Little and C. R. Dunstan, *Biomaterials*, 2010, **31**, 3175-3184.
29. S. Miao, K. Cheng, W. Weng, P. Du, G. Shen, G. Han, W. Yan and S. Zhang, *Acta Biomater*, 2008, **4**, 441-446.
31. K. Indira, U.K. Mudali, and N. Rajendran, *Journal of biomaterials applications*, 2013, **16**.
32. H. Hu, W. Zhang, Y. Qiao, X. Jiang, X. Liu and C. Ding, *Acta Biomater*, 2012, **8**, 904-915.
33. R.K. Dutta, B.P. Nenavathu, M.K. Gangishetty, and A.V. Reddy *Colloids and surfaces B, Biointerfaces*, 2012, **94**, 143-150.
34. W. Lin, V. Xu, C. C. Huang, Y. Ma, K. B. Shannon, D. R. Chen and Y. W. Huang, *J Nanopart Res* 2009, **11**.
35. G. M. Bishop, R. Dringen and S. R. Robinson, *Free Radic Biol Med*, 2007, **42**, 1222-1230.
36. K.R. Raghupathi, R.T. Koodali, and A.C. Manna. *Langmuir*, 2011, **27**, 4020-4028.
37. T. Xia, M. Kovochich, M. Liong, L. Mädler, B. Gilbert, H. Shi, J. I. Yeh, J. I. Zink and A. E. Nel, *ACS Nano*, 2008, **2**, 2121-2134.
38. H. L. Karlsson, P. Cronholm, J. Gustafsson and L. Möller, *Chem Res Toxicol*, 2008, **21**, 1726-1732.
39. A. Gojova, B. Guo, R. S. Kota, J. C. Rutledge, I. M. Kennedy and A. I. Barakat, *Environ Health Perspect*, 2007, **115**, 403-409.
40. C. Dong and F. Q. Zhang, *J Oral Rehabil*, 2009, **36**, 894-901.
41. M. A. Vargas-Reus, K. Memarzadeh, J. Huang, G. G. Ren and R. P. Allaker, *Int J Antimicrob Agents*, 2012, **40**, 135-139.

42. H. Koo, J. Seils, J. Abranches, R. A. Burne, W. H. Bowen and R. G. Quivey, *Antimicrob Agents Chemother*, 2006, **50**, 542-546.
43. H. Koo, P. L. Rosalen, J. A. Cury, Y. K. Park and W. H. Bowen, *Antimicrob Agents Chemother*, 2002, **46**, 1302-1309.
44. H. Koo, J. Sheng, P. T. Nguyen and R. E. Marquis, *FEMS Microbiol Lett*, 2006, **254**, 134-140.
45. J. A. Banas and M. M. Vickerman, *Crit Rev Oral Biol Med*, 2003, **14**, 89-99.
46. T. N. Phan, T. Buckner, J. Sheng, J. D. Baldeck and R. E. Marquis, *Oral Microbiol Immunol*, 2004, **19**, 31-38.
47. S. Oh, K. S. Brammer, Y. S. J. Li, D. Teng, A. J. Engler, S. Chien and S. Jin, *P Natl Acad Sci USA*, 2009, **106**, 2130-2135.
48. G. R. Sauer and R. E. Wuthier, *Bone and Mineral*, 1992, **17**, 284-289.
49. M. Lai, K. Cai, L. Zhao, X. Chen, Y. Hou and Z. Yang, *Biomacromolecules*, 2011, **12**, 1097-1105.
50. C. J. Van Oss, R. F. Giese Jr. and R. J. Good, *Langmuir*, 1990, **6**, 4.
51. N. Wang, H. Li, J. Wang, S. Chen, Y. Ma and Z. Zhang, *ACS appl mater inter*, 2012, **4**, 4516-4523.

Figure 1

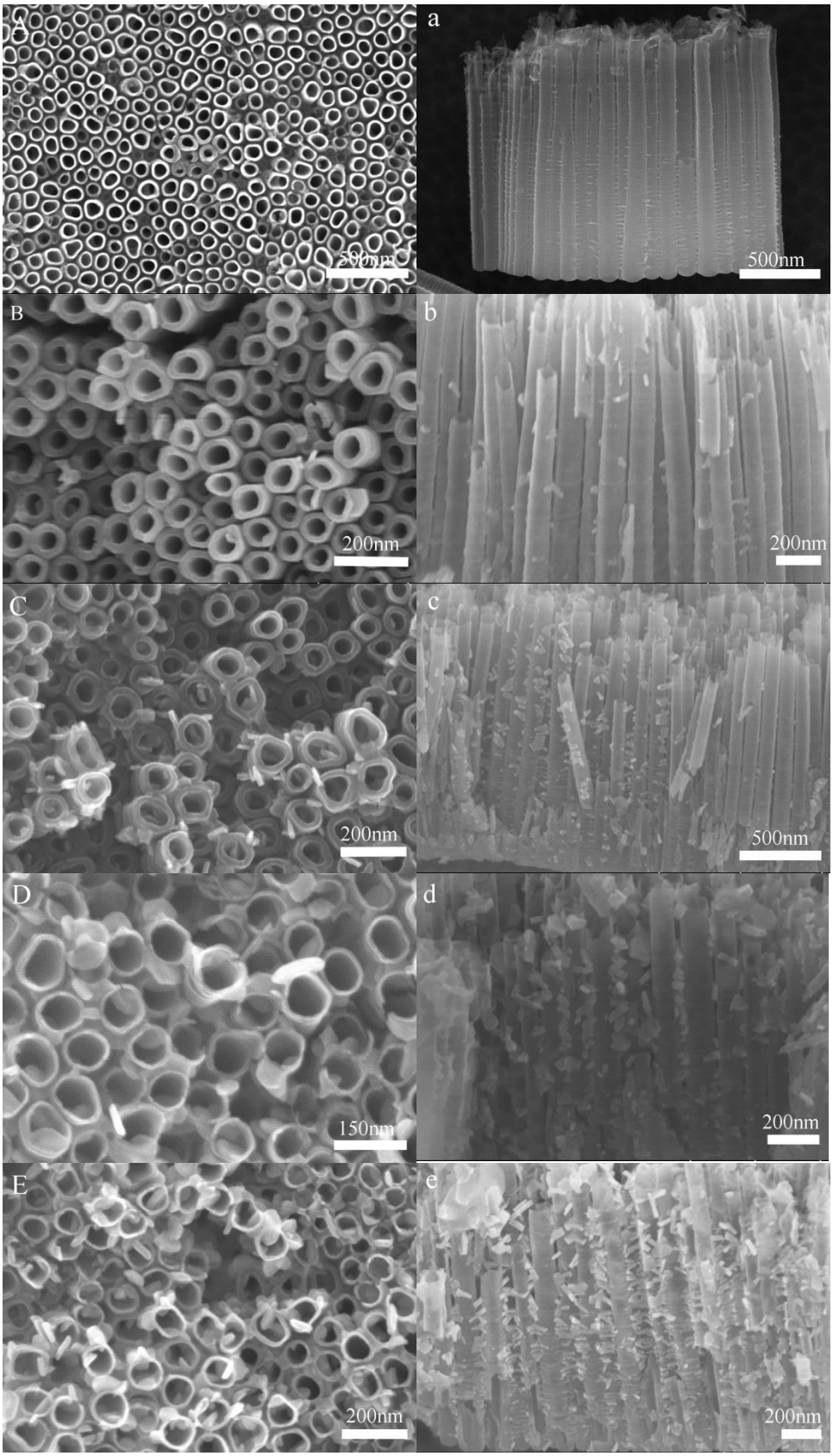

Figure 1. SEM images of the samples (titanium nanotubes is TNT, Zn-decorated TNTs is termed TNT-Zn): (A,a) TNT, (B,b) TNT-Zn0.005, (C,c) TNT-Zn0.015, (D,d) TNT-Zn0.030 and (E,e) TNT-Zn0.075.

Figure 2

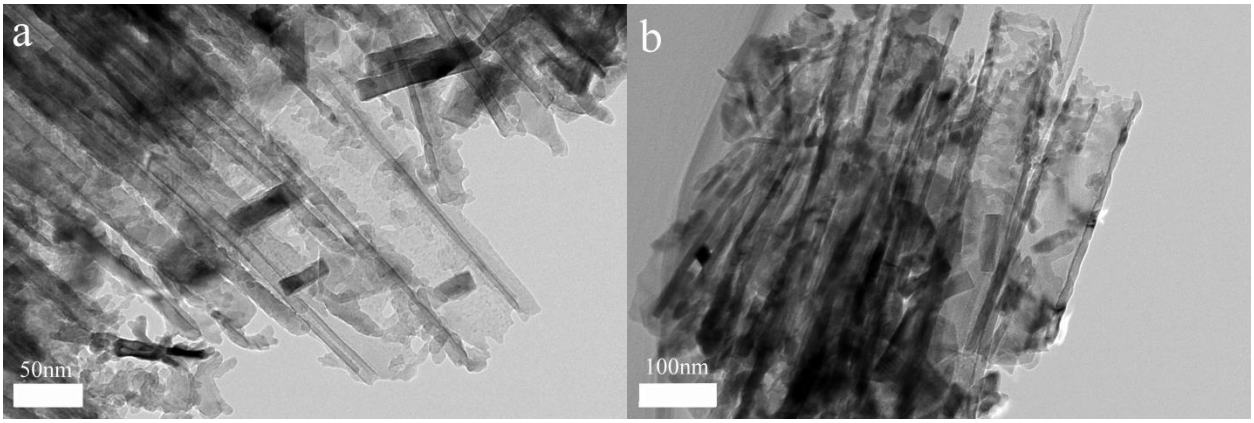

Figure 2. TEM image of TNT-Zn0.015.

Figure 3

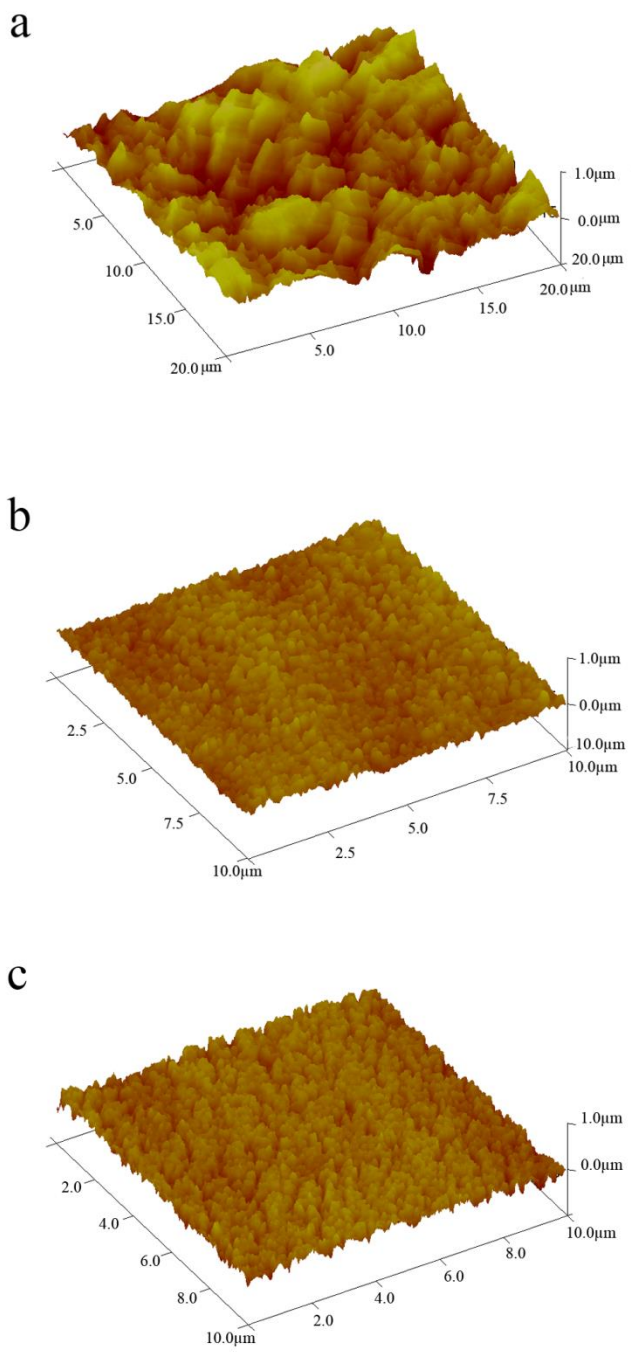

Figure 3. AFM images of samples: (a) Ti, (b) TNT, and (c) TNT-Zn0.015.

Figure 4

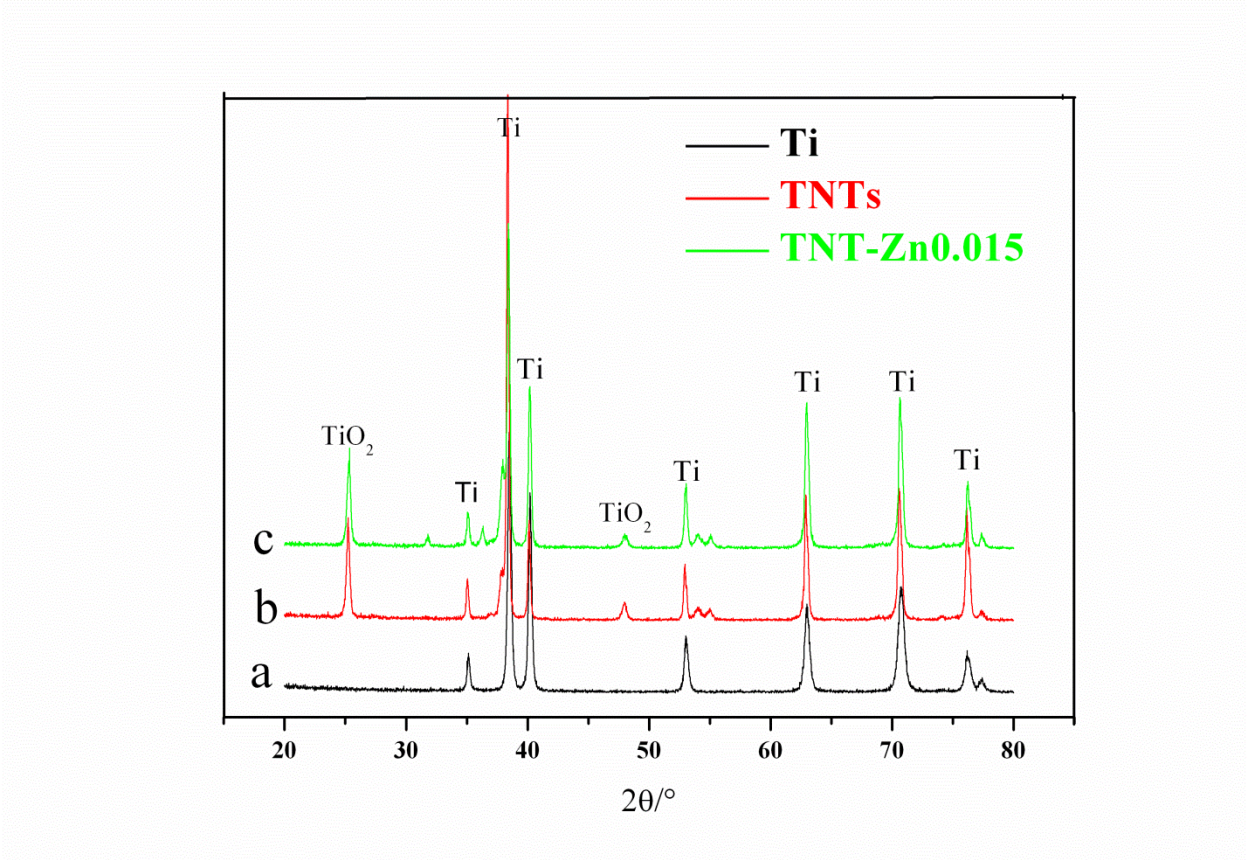

Figure 4. XRD patterns of Ti, TNTs and TNT-Zn0.015.

Figure 5

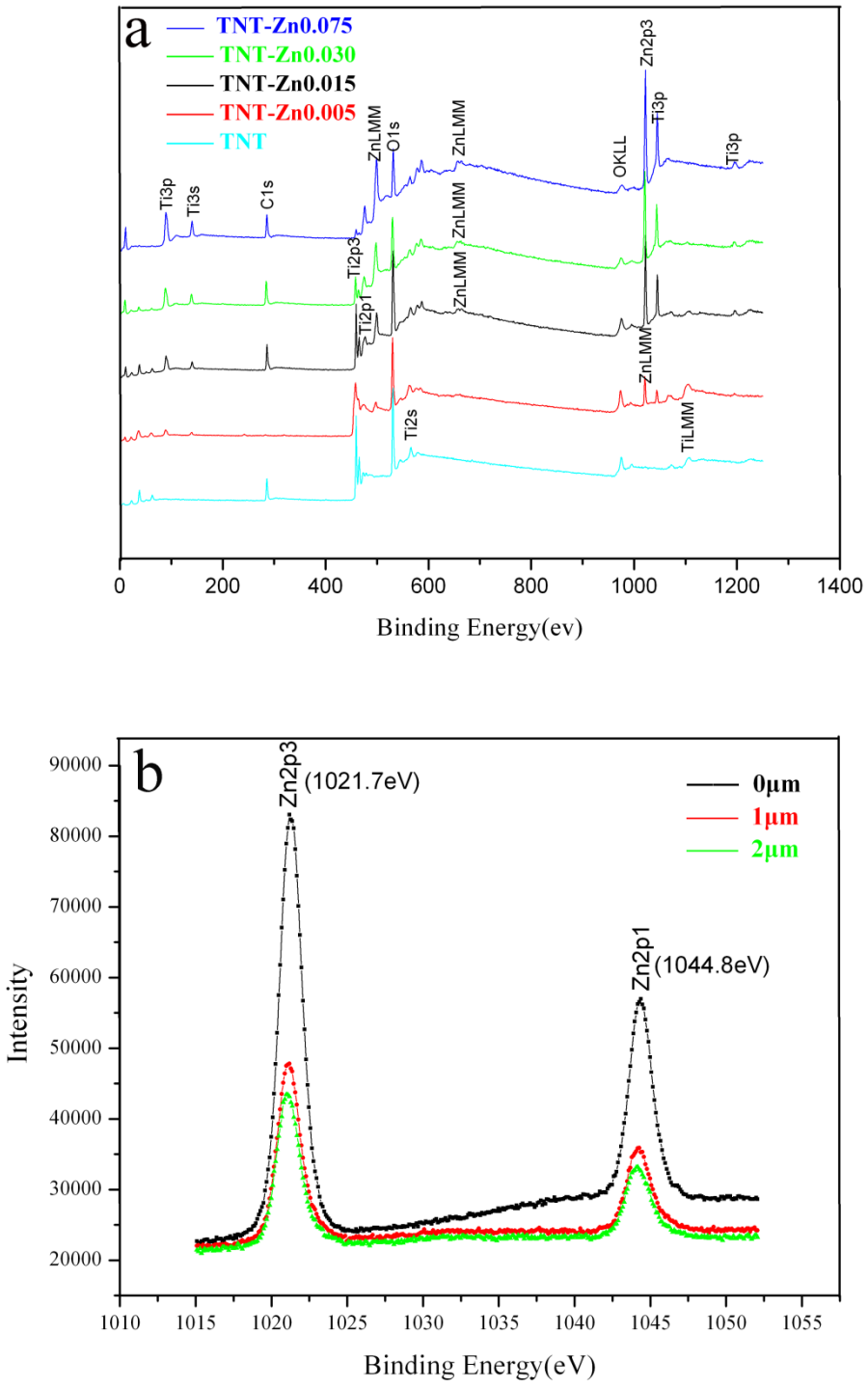

Figure 5. (a) XPS spectra of samples and (b) High-resolution XPS spectra of Zn2p at different depths in TNT-Zn0.015.

Figure 6

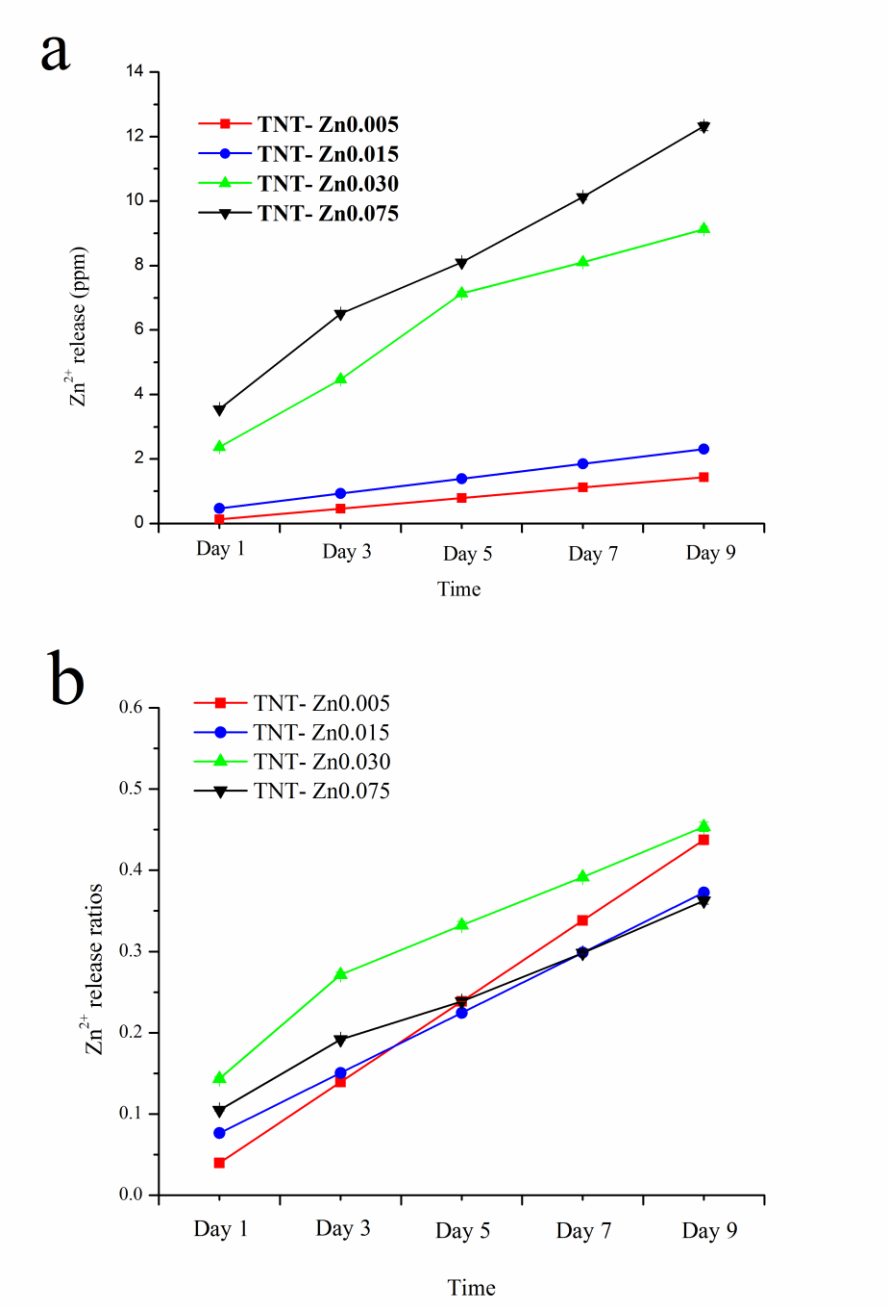

Figure 6. Zn release profiles of the Zn decorated samples: (a) Accumulated concentration of Zn^{2+} release and (b) Zn^{2+} release concentrations / total Zn^{2+} concentration in samples.

Figure 7

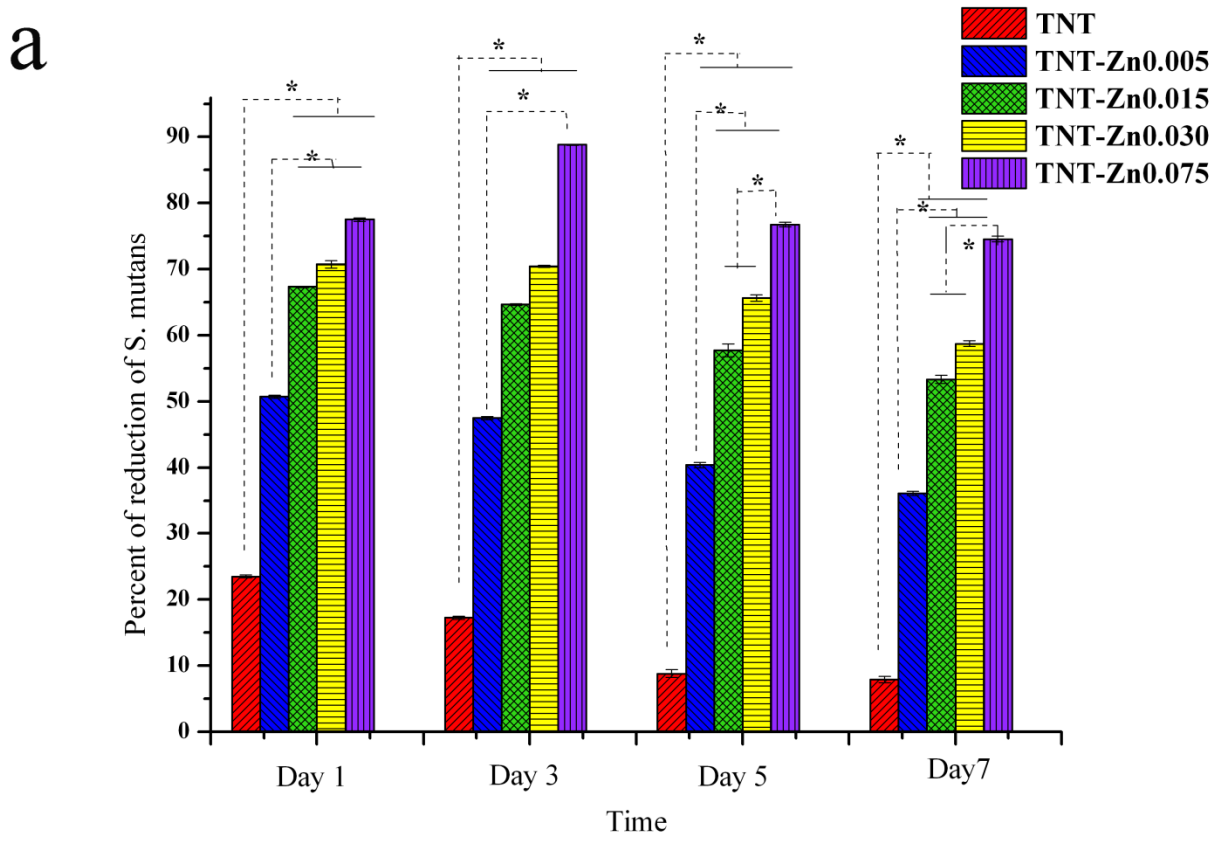

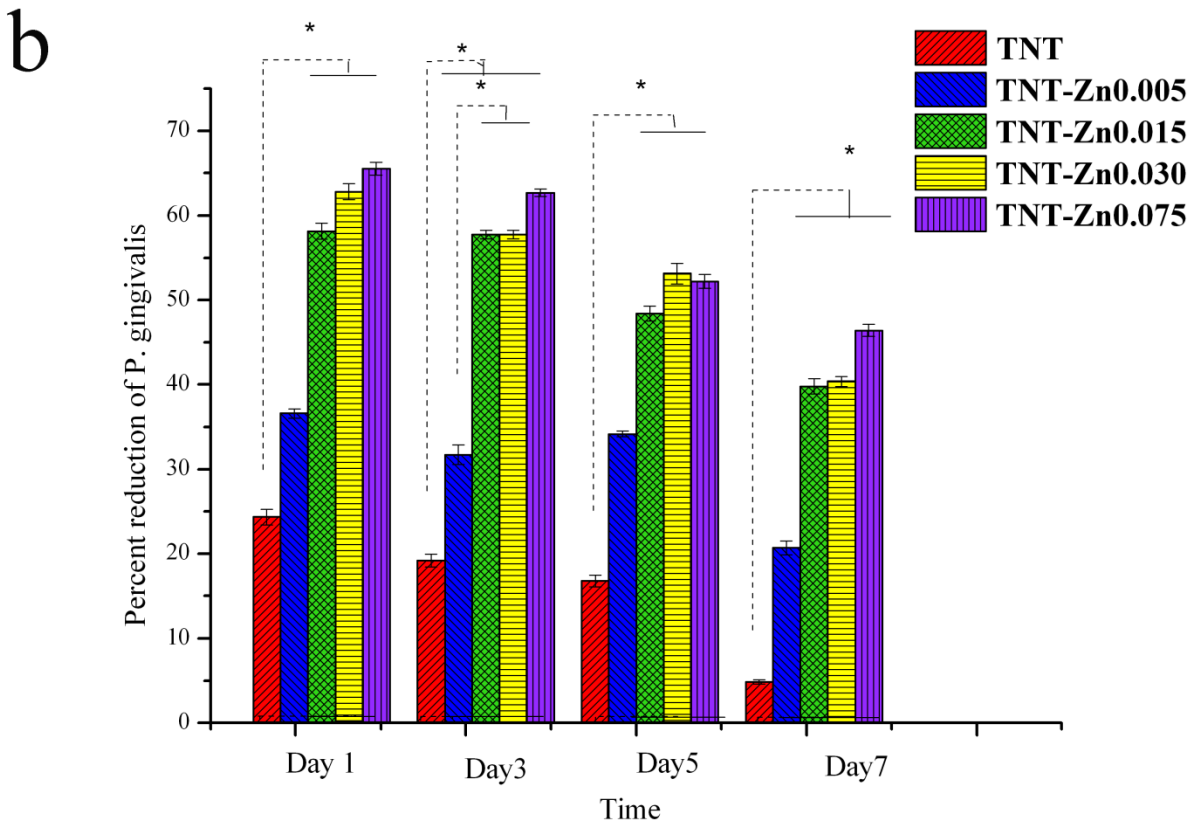

Figure 7. (a) *S. mutants* reduction rates on experimental samples and (b) *P. gingivalis* reduction rates on experimental samples. Antibacterial assay data are expressed as the mean ± standard deviation; (n=3); * $p<0.05$.

Figure 8

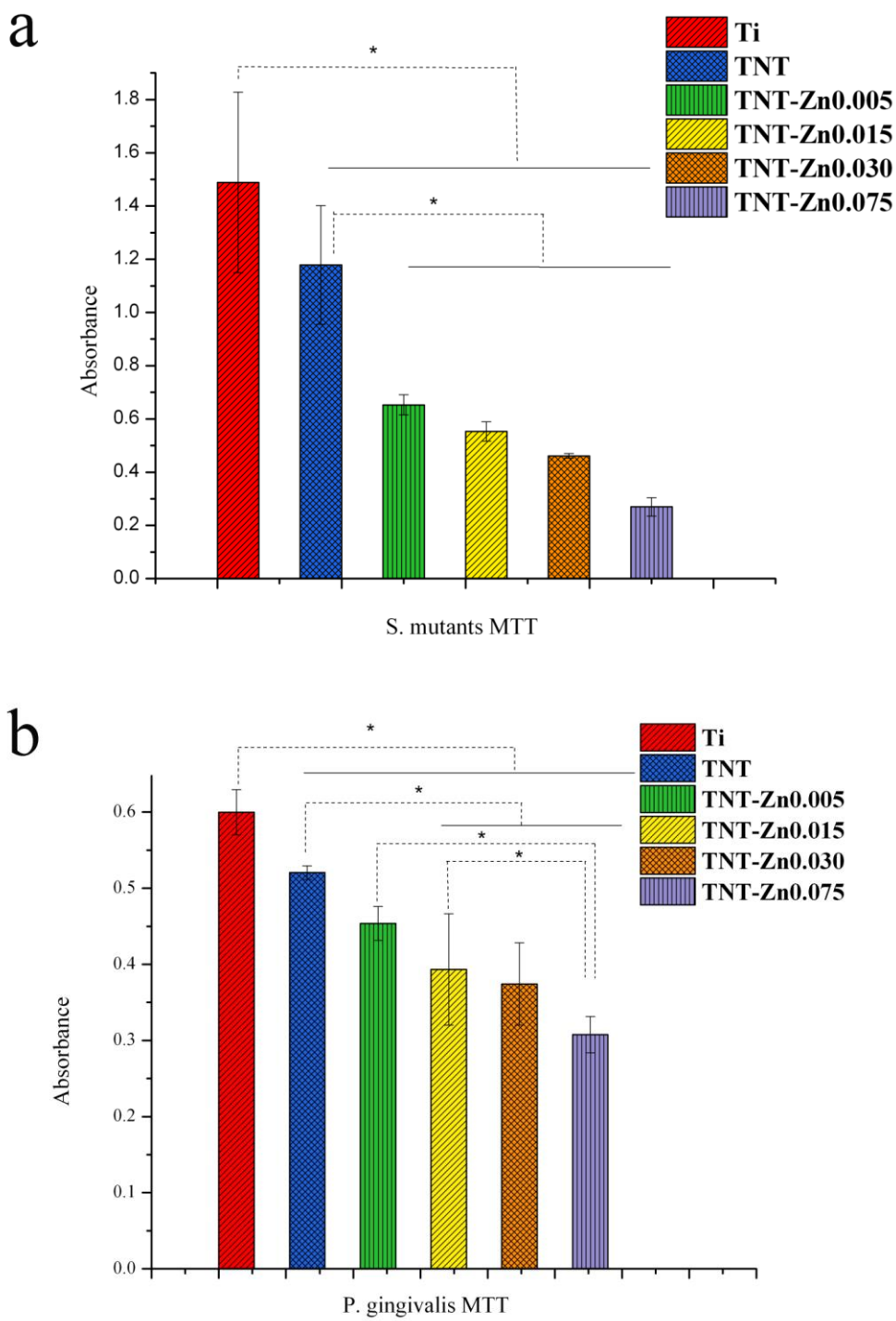

Figure 8. (a) MTT of *S. mutants* showed that there were significant differences between all Zn decorated TNT and Ti ($p<0.05$). (b) MTT for *P. gingivalis* showed that the experimental groups had significant differences with the control groups. Antibacterial assay data are expressed as the mean ± standard deviation; (n=3); * $p<0.05$.

Figure 9

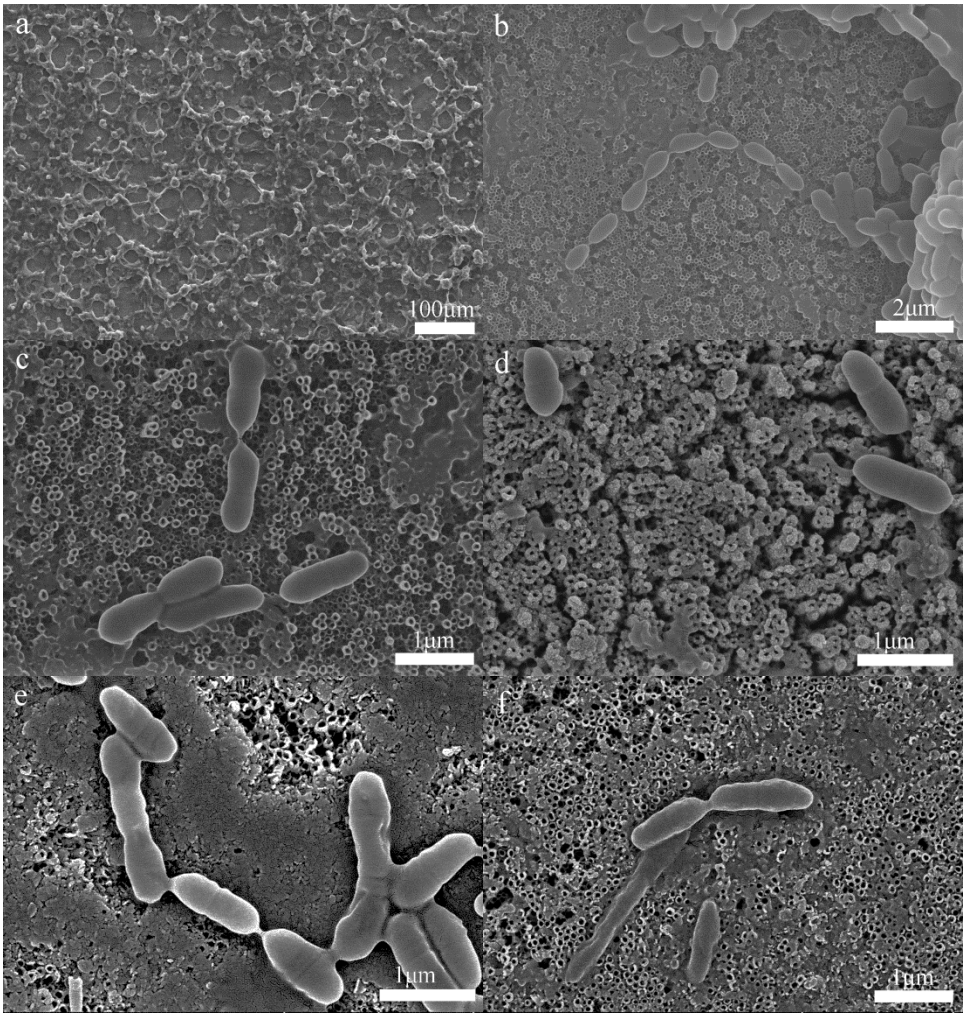

Figure 9. SEM images of *S. mutants* on samples: (a) Ti, (b) TNT, (c) TNT-Zn0.005, (d) TNT-Zn0.015, (e) TNT-Zn0.030 and (f) TNT-Zn0.075.

Figure 10

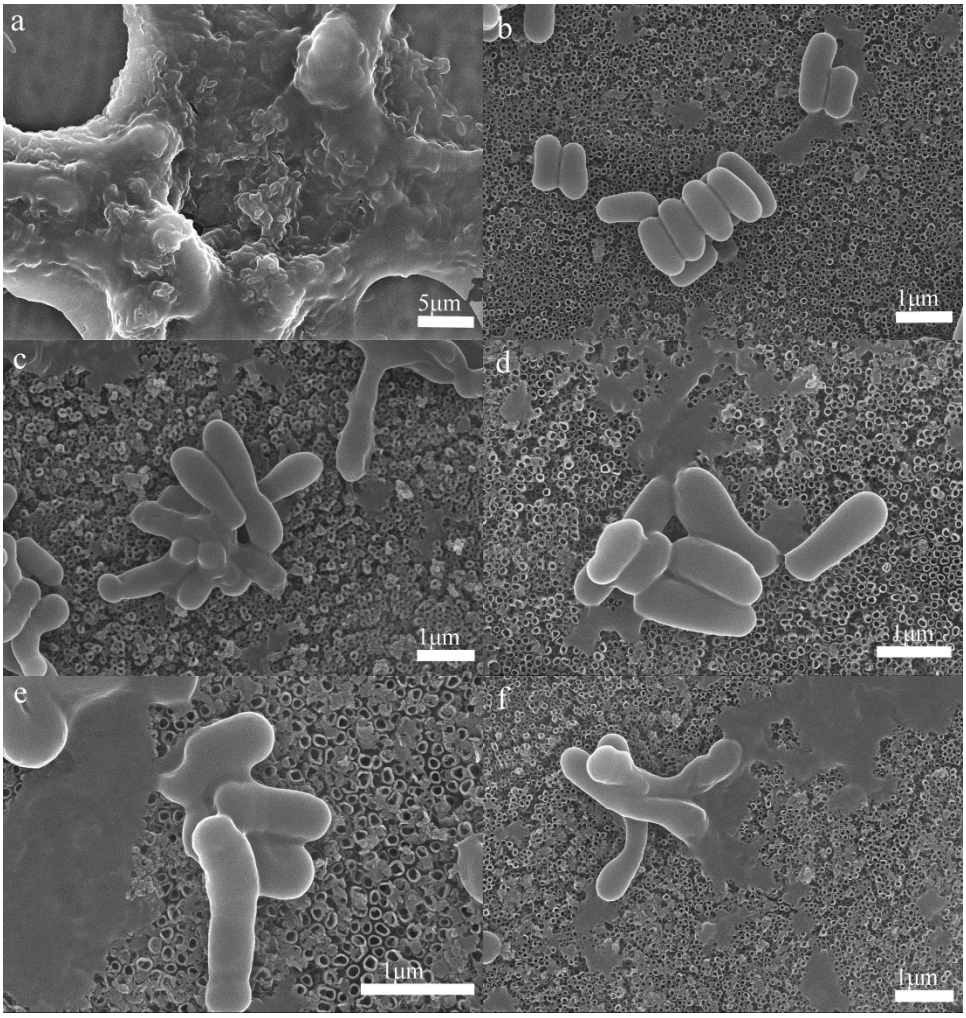

Figure 10. SEM image of *P. gingivalis* on samples: (a) Ti, (b) TNT, (c) TNT-Zn0.005, (d) TNT-Zn0.015, (e) TNT-Zn0.030 and (f) TNT-Zn0.075.

Figure 11

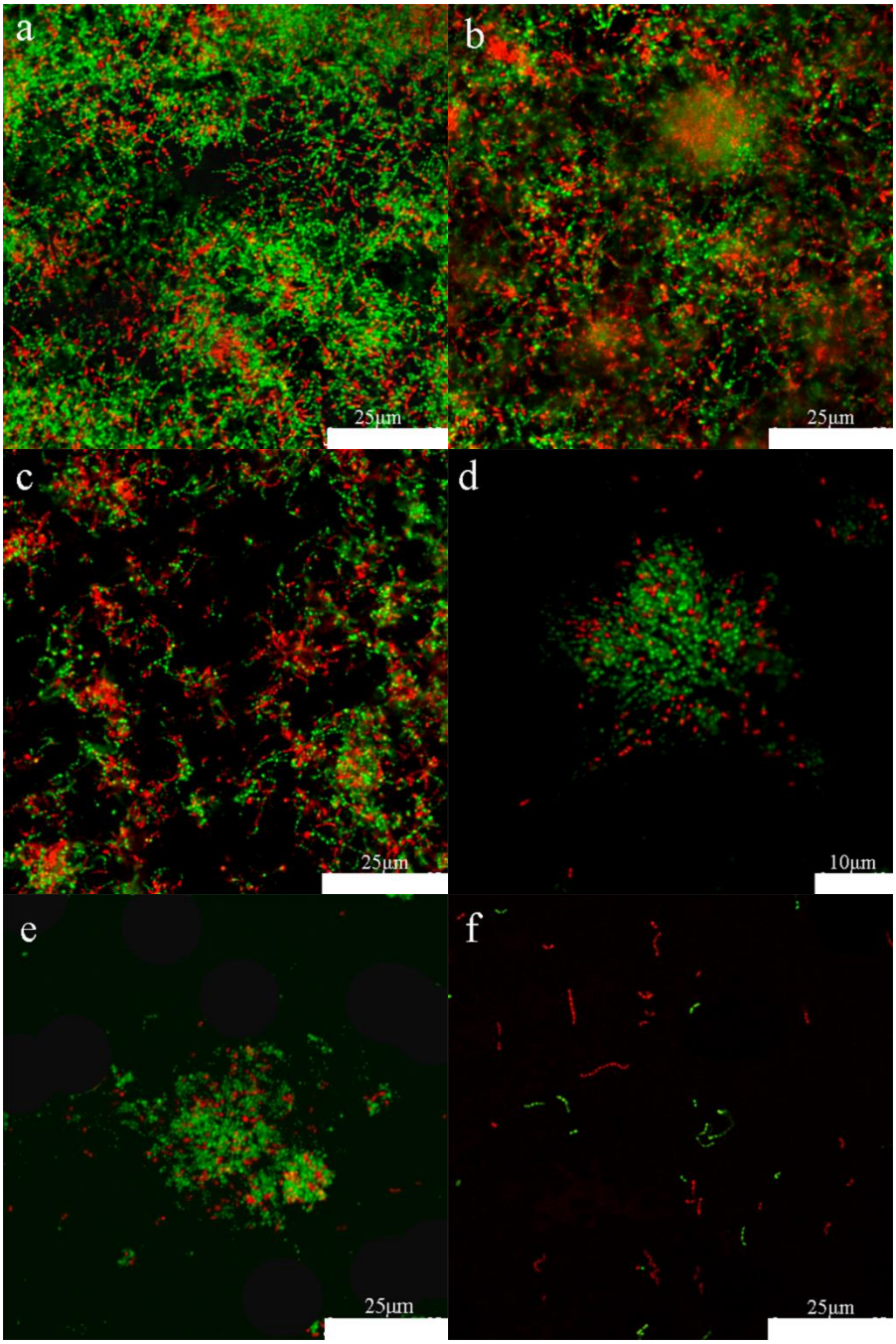

Figure 11. Fluorescence images showing the viability of the *S. mutants* on samples: (a) Ti, (b) TNT, (c) TNT-Zn0.005, (d) TNT-Zn0.015, (e) TNT-Zn0.030 and (f) TNT-Zn0.075. The live bacteria appear green while dead ones are orange.

Figure 12

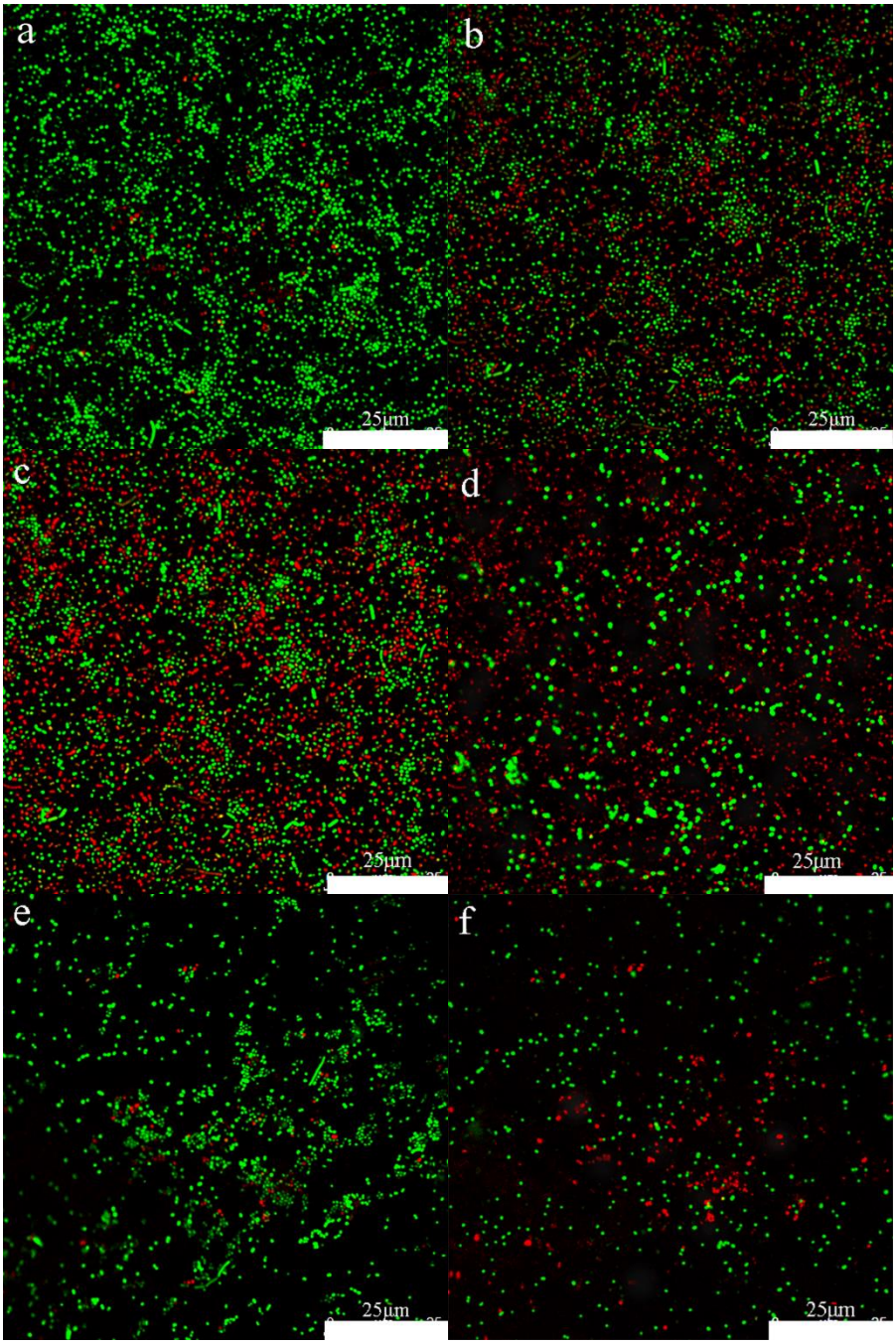

Figure 12. Fluorescence images showing the viability of the *P. gingival* on samples: (a) Ti, (b) TNT, (c) TNT-Zn0.005, (d) TNT-Zn0.015, (e) TNT-Zn0.030 and (f) TNT-Zn0.075. The live bacteria appear green while dead ones are orange.

Figure 13

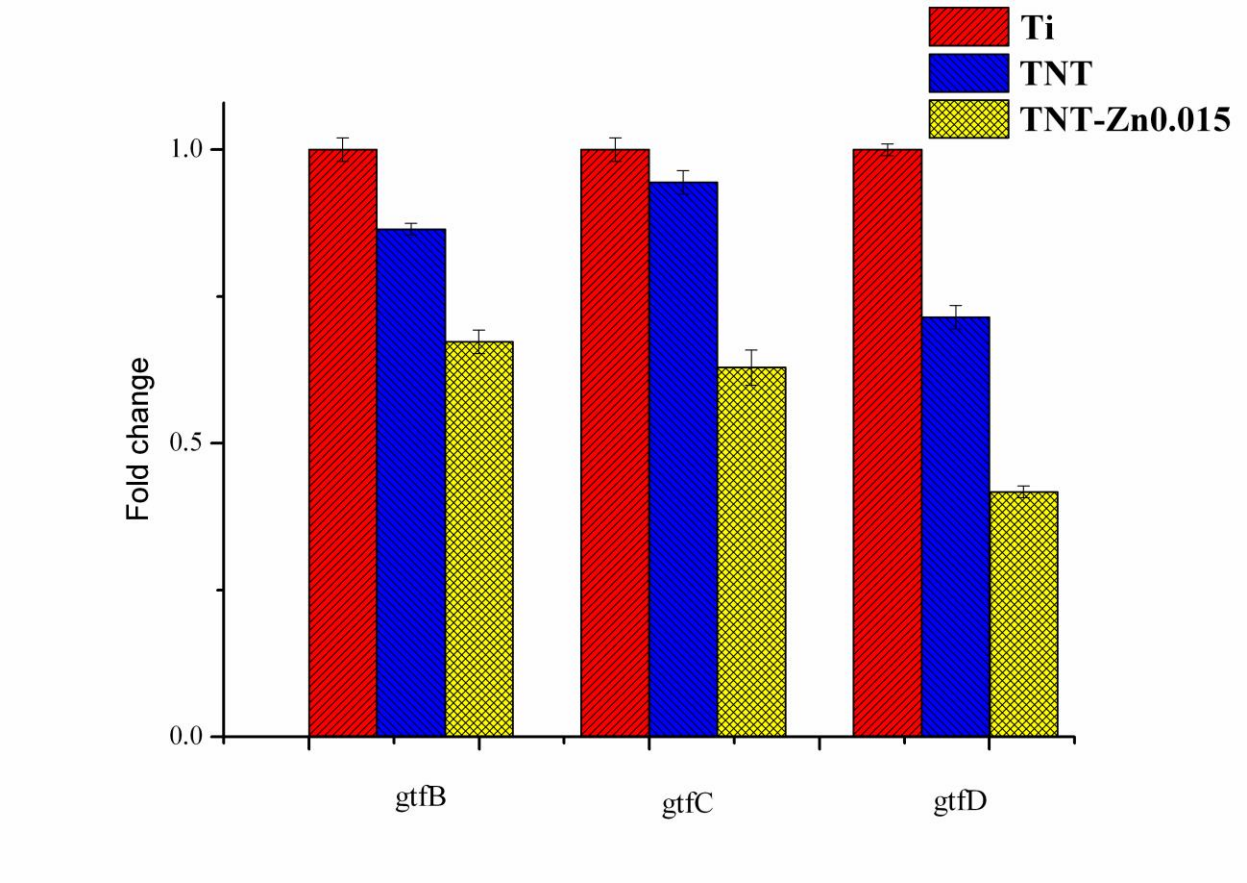

Figure 13. *S. mutants* adhesive gene expression on Ti, TNT and TNT-Zn0.015. There were significant differences in genes expression of gtfB, gtfC and gtfD. Antibacterial assay data are expressed as the mean ± standard deviation; (n=3); * $p<0.05$.

Figure 14

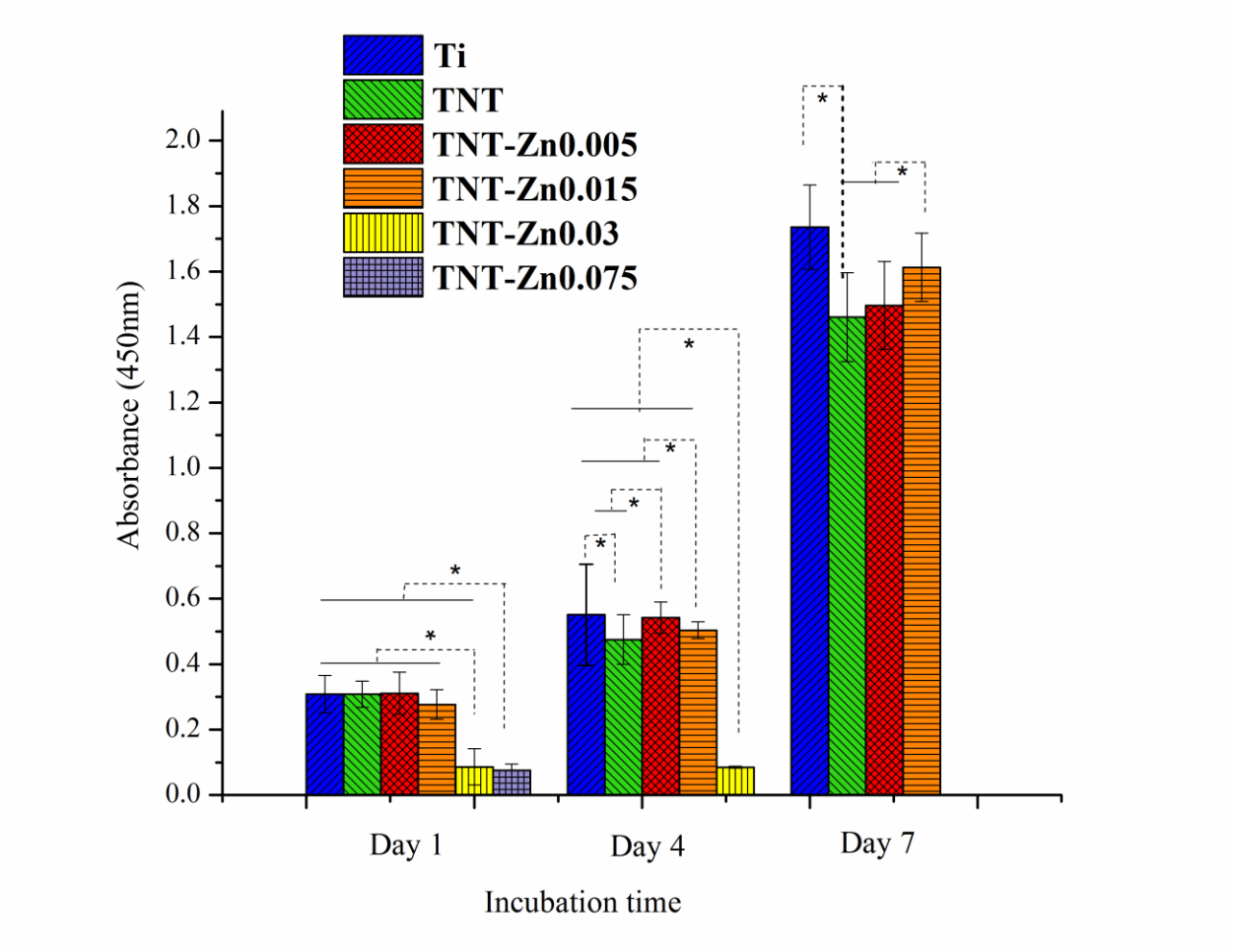

Figure 14. Stem cells proliferation on samples. CCK8 result of stem cells culture for 1, 4 and 7 days. Data are expressed as the mean ± standard deviation; (n=3); *p<0.01.

Fiugre 15

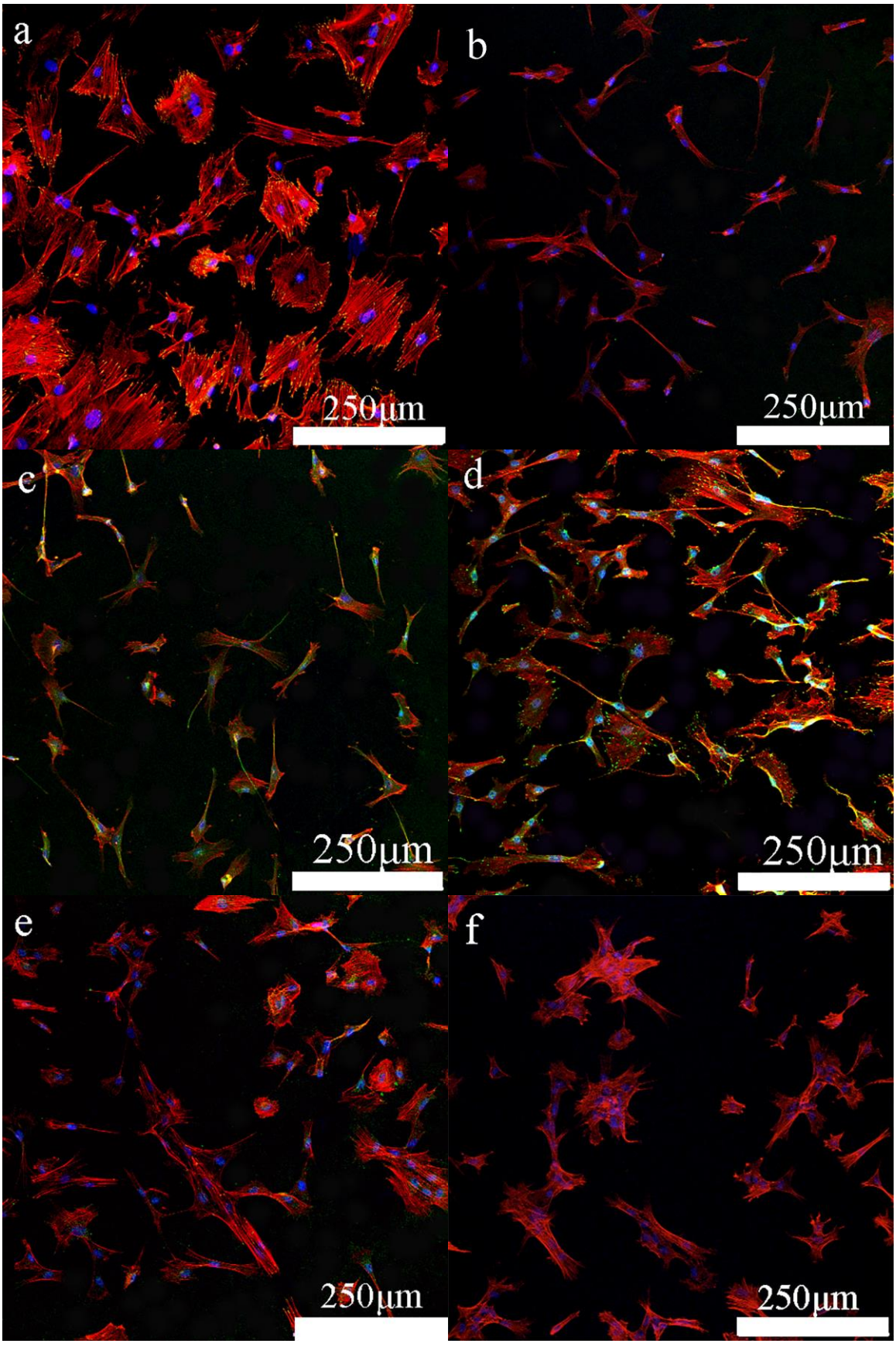

Figure 15. Flouorochrome micrography of stem cells cultured for 24 h on (a) Ti, (b) TNT, (c) TNT-Zn0.005, (d) TNT-Zn0.015, (e) TNT-Zn0.030, and (f) TNT-Zn0.075. Actin (red), Vinculin (green), and cell nucleus (blue).